Geol. Mag. **134** (*1*), *1997. pp. 99–112.*

Tectonic fingerprints in siderite cement, Tirrawarra Sandstone, southern Cooper Basin, Australia

M. R. REZAEE*, N. M. LEMON* & R. J. SEGGIE†

* National Centre for Petroleum Geology & Geophysics, University of Adelaide, South Australia, 5005, Australia
† Santos Ltd., 101 Grenfell Street, Adelaide, S.A. 5000, Australia

(*Received* 2 February 1996; *accepted* 18 July 1996)

Abstract – Compositional zoning and dissolution in cement is a direct response to the fluctuation of pore water chemistry, the variation of which during burial can be controlled by many factors, including the interaction between pore water and rock-forming minerals and the mixing of fluids from different origins. This paper suggests that tectonic activity can, by altering the hydraulic gradient, also influence pore water chemistry and lead to dissolution of cement, made clear by zoning within siderite crystals. Three different stages of siderite cement have been described from the Tirrawarra Sandstone in the Moorari and Fly Lake fields of the southern Cooper Basin, here referred to as S1 (early), S2 (middle), and S3 (late). Ragged dissolution surfaces separate the main phases, occurring after precipitation of S1 and S2 with incipient dissolution suggested within S2. Back-scattered electron (BSE) images and electron microprobe analyses clearly differentiate each main phase of siderite. S1 is a homogeneous, iron-rich siderite whereas S2 displays patchy compositional zoning associated with several minor dissolution stages, and S3 commences with even compositional banding and grades into a thick homogeneous phase in the terms of composition.

Isotope analyses and fluid inclusion studies indicate that S1 formed at a temperature around 30 °C, S2 precipitated at a minimum temperature of 68 °C, and S3 formed around 102 °C. The heterogeneous, pitted and zoned S2 is thought to have formed during a time of active tectonism in the Cooper Basin, whereas the evenly banded nature of S3 suggests that it precipitated during a quiet tectonic period when pore waters largely remained relatively constant. It appears that siderite cements in the Tirrawarra Sandstone record tectonic activity in the form of irregular growth and dissolution highlighted by compositional zoning with stages of strong dissolution recording particularly active times when pore waters changed composition dramatically. Some zoning could be related in part to tectonic pulses. The temperature recorded by each of the siderite stages allows their precipitation to be tied to a burial history curve, and by making some simple assumptions about that history, the timing of cementation can be estimated. This can be a additional tool for calibrating the thermal history of an area.

1. Introduction

The results of this study indicate that authigenic minerals formed during burial diagenesis may record tectonic activity of a basin. Dissolution phases and possibly compositional zoning in a cement indicate fluctuation in pore fluid chemistry and may be related to tectonic activity. As siderite, unlike other carbonate minerals, does not undergo geochemical and isotope re-equilibration during burial diagenesis (Curtis, Pearson & Somogyi, 1975; Gautier, 1982; Pearson, 1985; Curtis & Coleman, 1986), and there exists no documented case of siderite recrystallization (Mozley & Carothers, 1992), siderite can be a powerful tool in recording basin events.

In the present investigation, different siderite cement stages are considered to be precipitated under different conditions in terms of tectonic activity in the late Carboniferous–early Permian Tirrawarra Sandstone of the Moorari and Fly Lake fields, Cooper Basin, South Australia (Fig. 1). The data are based on the integration of petrographic, electron microprobe and back-scattered electron (BSE) images, fluid inclusion and stable isotope techniques. The data show that variation in the character of siderite cement is due to variation in cement composition which in turn is a function of fluctuation of pore water chemistry in Fe and Mg content. Rapid variation of pore water composition has resulted in irregular compositional zoning in siderite with obvious dissolution likely to be contemporaneous with the peak of tectonic activity in the Cooper Basin about 200 Ma. Siderite cement with relatively even banding or a homogeneous nature is considered to have formed during passive times in the Cooper Basin in terms of tectonic activity.

2. Geological and tectonic setting

The intracratonic Cooper Basin in Central Australia (Fig. 1) is Australia's largest onshore hydrocarbon province (Heath, 1989). The basin consists of dominantly lacustrine-fluvial deposits with local glacio-fluvial and rare periglacial aeolian sediments (cf. Kapel, 1966, 1972; Gatehouse, 1972; Battersby, 1976; Thornton, 1979; Stuart, 1976; Williams, Wild & Suttill, 1985; Fairburn, 1989). The basin is underlain by the early Palaeozoic marine and volcanic rocks of the Warburton Basin (Gatehouse, 1986) and overlain by the Jurassic–Cretaceous sediments of the Eromanga Basin (Exon & Senior, 1976; Armstrong & Barr, 1986). The basin is

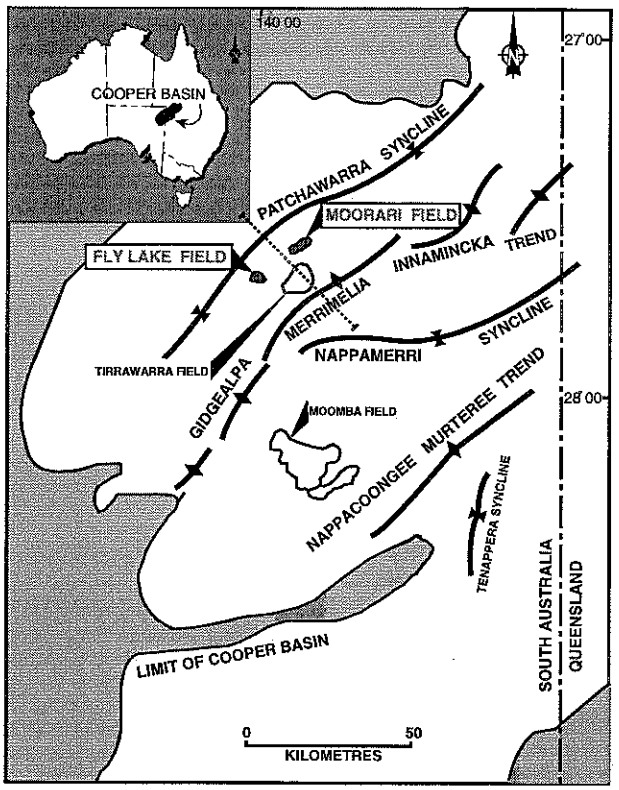

Figure 1. Location and map of the southern Cooper Basin showing the major structural elements and the location of the Moorari and Fly Lake fields in the Patchawarra Syncline (modified from Stuart, Kennedy & Thomas, 1988).

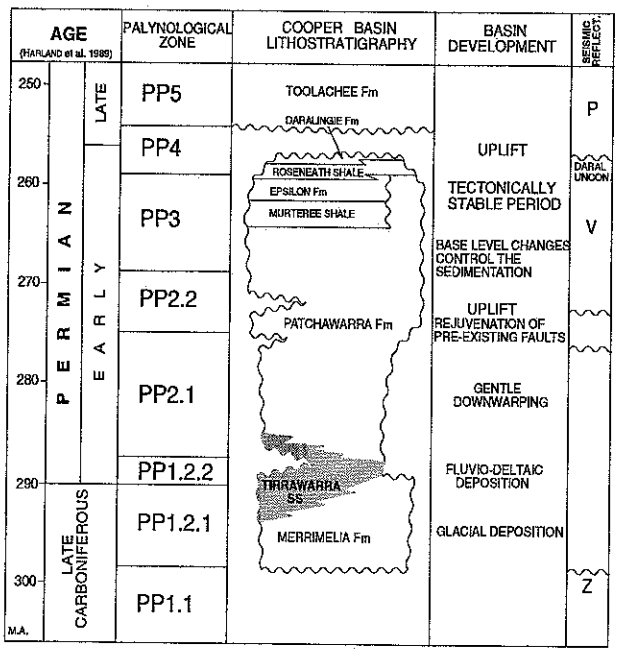

Figure 2. Stratigraphic column for the southern Cooper Basin with the main tectonic events. The fluvio-deltaic Tirrawarra Sandstone was deposited during the early subsidence history of the Cooper Basin when Australia was at high latitudes (modified from Apak, Stuart & Lemon, 1993 and Seggie *et al.* 1994).

characterized by three elongate depocentres, namely the Patchawarra, Nappamerri and Tenappera troughs, now folded as synclines, which are separated by the Gidgealpa–Merrimelia–Innamincka (GMI) and Murteree–Nappacoongee (MN) anticlinal trends (Fig. 1) (Thornton, 1979). The synclinal areas contain up to 1300 m of Permian sediments overlain by as much as 2500 m of Jurassic to Tertiary strata (Battersby, 1976; Thornton, 1979). Fluvial sandstones, which occur at various levels within the Permian section, are the main petroleum reservoirs and include the fluvio-glacial Tirrawarra Sandstone (Smyth, 1979; Kantsler *et al.* 1983; Heath, 1989; Hunt, Heath & Mckenzie, 1989; Yew & Mills, 1989). About 95% of the Cooper Basin oil is reservoired in the Tirrawarra Sandstone of the Tirrawarra Field (Heath, 1989; Seggie *et al.* 1994) (Fig. 2). Additional oil reserves occur at the same stratigraphic interval in the Moorari and Fly Lake fields (Fig. 1). The two fields were discovered in 1971 and are fault-bounded anticlinal structures. In both fields, the Tirrawarra Sandstone reservoirs are characterized by relatively low porosities (9 to 12%), low permeabilities (0.1 to 15 mD *in situ*) and hence relatively low productivities (25 to 600 BOPD) (Rodda & Paspaliaris, 1989; Yew & Mills, 1989).

Several tectonic events occurred during and after deposition of the Tirrawarra Sandstone. Some of the tectonic events are minor, such as the one which occurred during the Tirrawarra Sandstone deposition (T0a), and some of them are major tectonic events (T1 to T3). Apak, Stuart & Lemon (1993) documented another weak tectonic event within the Patchawarra Formation (here referred to as T0b). This event is seen as local truncation of section over the GMI Trend but fades towards the depocentres, including the study area. The main tectonic events are highlighted in a seismic section near the study area (Fig. 3) and a regional cross-section (Fig. 4) from Kreig, Alexander & Rogers (1995).

The first main tectonic event (T1) after deposition of the Tirrawarra Sandstone occurred in the form of uplift and erosion after deposition of the Daralingie Formation (Thornton, 1979). Compressive forces reactivated basement thrusts resulting in an angular contact between the Toolachee Formation and various underlying formations (Wopfner, 1966; Kapel, 1972; Pyecroft, 1973; Thornton, 1979). The erosion is particularly apparent over the GMI trend (Apak, Stuart & Lemon, 1993) and is strong enough to be present in the study area in the middle of the Patchawarra Trough (Hill & Gravestock, 1995) but may be less prominent in the deeper Nappamerri Trough to the east of the GMI ridge. A hiatus in sedimentation of about 12 Ma at the end of early Permian time is recorded by palynological studies (Thornton, 1979).

Cooper Basin deposition terminated before the end of Triassic time when widespread folding, regional uplift and erosion, here referred to as event T2, occurred (Battersby, 1976). Compression again reactivated the main basement faults (Apak, Stuart & Lemon, 1993) but the main effect of this event was to tilt the basin to the

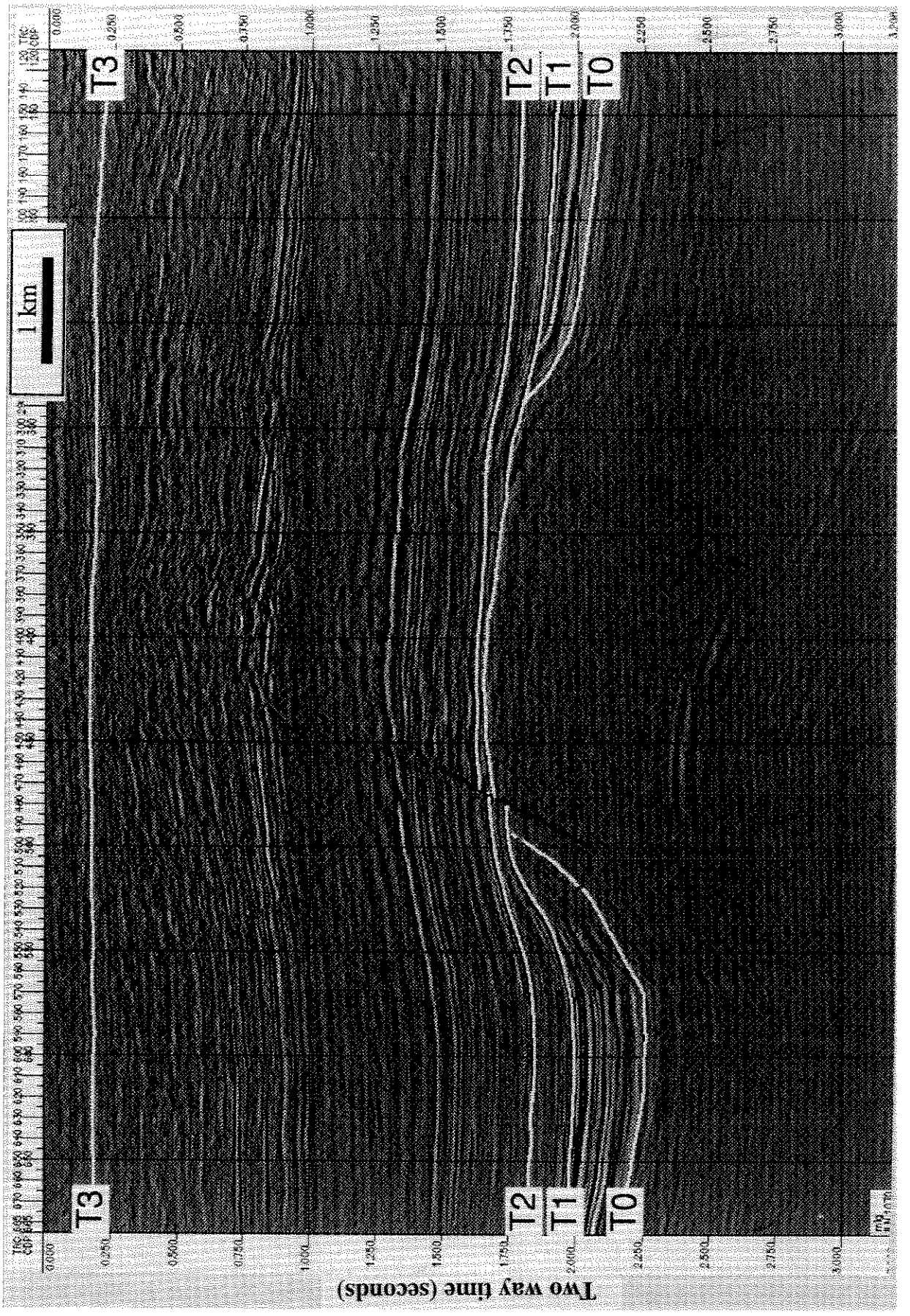

Figure 3. Interpreted seismic section from near the study area (see Fig. 1 for location), highlighting the tectonic events. T0, a minor event, occurred during deposition of the Tirrawarra Sandstone. T1, T2 and T3 are major events which occurred after deposition of the Tirrawarra Sandstone. Associated uplift and erosion is most prominent over the basement ridge, but the events have been documented into the Patchawarra Syncline.

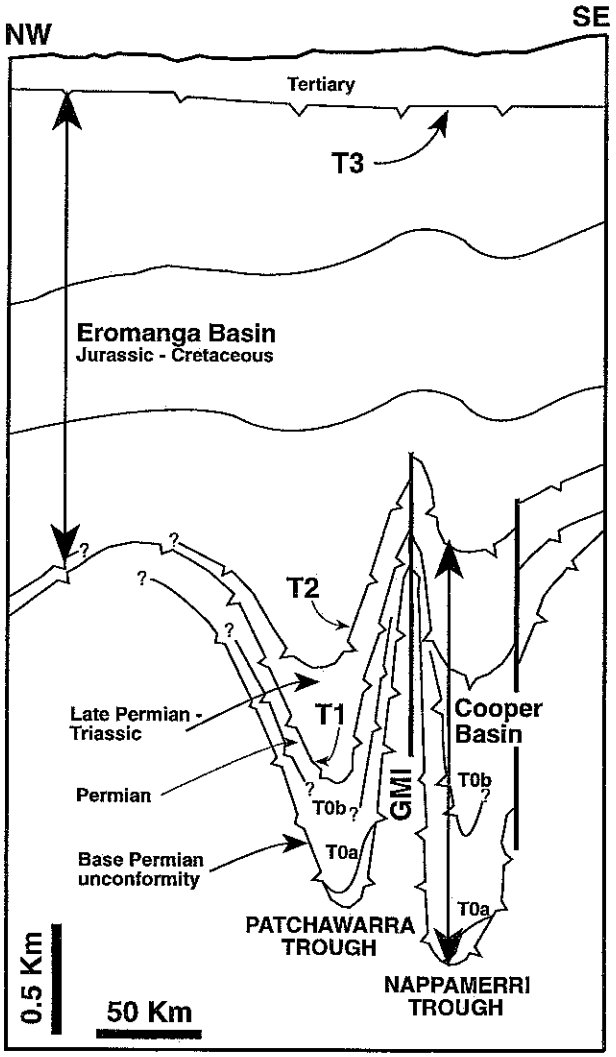

Figure 4. Schematic cross-section from the Patchawarra Syncline, over the GMI Ridge and into the Nappamerri Syncline illustrating the position of the main unconformities in the area. GMI is Gidgealpa–Merrimelia–Innamincka Ridge (modified from Kreig, Alexander & Rogers, 1995).

northeast, thereby dramatically separating the Permian and Triassic depocentres. Up to 500 m erosion of sediments has been recognized in the southern parts of the basin (Kantsler *et al.* 1983; Gray & Roberts, 1984), and although the effect diminished to the north, erosion is still evident in the study area.

Deposition of Eromanga Basin sediments (Jurassic–Cretaceous) commenced on the erosion surface of the Cooper Basin (Kantsler *et al.* 1983; Heath, 1989). After a rapid subsidence which allowed deposition of the Cretaceous section, another tectonic event (T3) resulted in folding and faulting (Heath, 1989).

3. Methods of study

A total of 130 core samples were collected from 14 wells in the Moorari and Fly Lake fields. Detailed sedimentological descriptions of the cores were carried out and a variety of depositional environments were sampled. The samples were characterized using the following techniques.

3.a. Optical petrography

All samples were prepared either as normal thin or polished thin sections following impregnation of the samples with blue-dyed epoxy resin to facilitate the recognition of porosity. Micrographs were taken of all representative features. Quantitative estimates of sandstone mineralogy, texture and porosity were obtained by point-counting (400 to 600 counts per thin section).

3.b. Scanning electron microscopy (SEM)

SEM studies were carried out on selected core samples coated with carbon and gold/palladium using a Phillips XL20 electron microscope connected to a back-scattered electron (BSE) detector. Energy dispersive X-ray (EDX) analysis was employed to study the composition of representative authigenic minerals.

3.c. Electron microprobe analysis

Quantitative elemental composition of siderite cement was carried out on a CAMECA SX 51 microprobe at 15 kV, using a 20 nA beam current and a 0.2 μm beam diameter. The BSE imaging system linked to the electron microprobe was used to detect zonation in the siderite cement, and compositional analyses were carried out for each stage of siderite cement (Table 1).

3.d. Isotope analysis

Oxygen and carbon isotope analyses were carried out on 18 core samples following selection of the samples using optical and bulk XRD methods. Only samples containing major amounts of siderite that lacked other carbonate cement types were selected for stable isotope analysis. The samples were crushed to a fine dry powder and then reacted with 100% phosphoric acid under vacuum at 100 °C overnight (Rosenbaum & Sheppard, 1986). The resultant carbon dioxide was purified by the conventional techniques of McCrea (1950) and analysed on a 6-inch dual collector VG Micromass 602E mass spectrometer. The acid correction factors of Rosenbaum & Sheppard (1986) were used to compensate for the oxygen isotope fractionation. Stable isotope values are reported in the δ-notation in parts per thousand (‰). All oxygen isotope ratios are reported relative to standard mean ocean water (SMOW) (Craig, 1961), and all carbon isotope values relative to the *Bellemnitella americana* from the Pee Dee Formation (PDB) (Craig, 1957).

The integrated use of video-imaging and image analysis software introduced by Rezaee & Schulz-Rojahn (1996) provided an efficient means of quantifying the

Table 1. Microprobe results for the different siderite cement stages

Well name	Sample no.	FeO (%)	Mg (%)	Ca (%)	Mn (%)	Cement stage
Fly Lake 1	F1-9431	60.59	37.09	1.51	0.80	S2
	F1-9431	67.73	30.85	0.36	1.06	S2
	F1-9431	80.24	19.03	0.07	0.66	S3
	F1-9431	71.89	27.41	0.04	0.66	S3
	F1-9431	68.39	29.65	1.22	0.74	S3
	F1-9431	77.79	21.32	0.15	0.74	S3
Fly Lake 2	F2-9570	77.17	21.55	0.51	0.77	S3
	F2-9583	96.90	0.24	1.16	1.69	S1
	F2-9583	75.88	22.92	0.20	1.00	S2
Moorari 1	M1-9613	63.72	34.45	1.03	0.80	S2
	M1-9613	85.27	11.09	2.00	1.64	S2
	M1-9613	78.27	19.98	1.05	0.70	S2
	M1-9620	94.81	1.09	2.50	1.61	S1
	M1-9620	79.65	19.14	0.34	0.87	S2
Moorari 2	M2-10116	70.66	27.92	0.46	0.96	S2
	M2-10116	65.88	32.78	0.26	1.08	S2
	M2-10116	63.48	34.82	0.48	1.22	S3
	M2-10116	81.82	16.83	0.35	1.00	S3
	M2-10116	68.49	29.78	0.56	1.17	S3
	M2-10145	70.56	28.71	0.12	0.61	S2
	M2-10145	77.15	20.18	0.96	1.71	S2
	M2-10145	69.92	28.96	0.31	0.80	S2
	M2-10145	84.97	9.07	1.57	4.39	S3
	M2-10145	82.78	15.48	0.73	1.01	S3
Moorari 3	M3-9422	93.89	2.02	2.83	1.26	S1
	M3-9422	81.23	14.44	3.58	0.74	S2
	M3-9440	81.44	17.38	0.25	0.93	S2
	M3-9440	78.45	20.40	0.23	0.92	S3
	M3-9440	77.13	21.51	0.41	0.95	S3
	M3-9503	61.62	37.43	0.27	0.68	S2
	M3-9503	83.29	13.08	1.32	2.32	S2
	M3-9503	76.10	22.37	0.40	1.13	S2
Moorari 4	M4-9574	63.60	35.21	0.08	1.11	S2
	M4-9574	87.21	10.78	0.14	1.87	S2
	M4-9574	74.39	23.78	0.49	1.34	S2
	M4-9574	80.82	17.41	0.42	1.35	S3
	M4-9574	77.12	20.96	0.31	1.62	S3
Moorari 5	M5-9553	63.83	34.54	0.26	1.38	S2
	M5-9553	82.49	14.93	0.37	2.21	S2
	M5-9553	65.52	32.77	0.21	1.50	S2
	M5-9553	72.84	25.87	0.25	1.04	S3
	M5-9553	69.46	29.34	0.22	0.98	S3
Moorari 6	M6-9737	89.03	9.39	0.16	1.42	S3
	M6-9737	75.07	23.55	0.29	1.08	S3
	M6-9737	86.32	12.32	0.12	1.23	S3
Moorari 7	M7-9606	58.36	39.97	0.29	1.38	S2
	M7-9606	79.67	18.27	1.16	0.89	S2
Moorari 9	M9-9732	97.05	0.85	0.93	1.18	S1
	M9-9732	68.05	30.30	1.06	0.59	S2
	M9-9732	82.82	15.99	0.21	0.98	S2
	M9-9732	75.20	23.08	0.89	0.83	S2
	M9-9732	91.11	7.85	0.04	1.00	S3

S1 = early stage of siderite cement; S2 = middle stage of siderite cement; S3 = late stage of siderite cement.

different siderite cement generations seen under the BSE. The method provides for improved bulk-rock isotope interpretations in clastics containing multi-generation carbonate cements. Most of the samples selected were dominated by one of the siderite phases although a few contained mixtures of two dominant phases. Image analysis allowed accurate quantification of the amount of each phase present and plots of percentages of each phase against bulk isotope values enabled the determination of end-member $\delta^{18}O$ and $\delta^{13}C$ compositions of individual cement generations.

3.e. Fluid inclusion analysis

Twelve samples were selected for fluid inclusion analysis. Cycling methods (Reynolds, 1978) were employed to carry out microthermometry on small primary fluid inclusions. The fluid inclusion analysis was carried out under a Leitz optical microscope with a warming–cooling Reynolds stage. In all of the samples, isolates of two-phase liquid–vapour fluid inclusions were present. As the size of the fluid inclusions was small, it was not possible to observe the final melting of the ice. The microthermometry measurement precision is estimated at ± 1 °C.

4. Palaeoenvironmental interpretations

Various environments of deposition are recognized in the Tirrawarra Sandstone, including lacustrine, parallel beach-barrier, back-barrier marsh with outwash beds, distal and medial braid-delta, meandering system and aeolian depositional environments. The lacustrine deposits include both upper- and lower-shoreface clastics. Parallel beach-barrier sandstones are chiefly medium-grained, well-sorted quartzarenites. Back-barrier marsh sediments consist of massive mudstones, fine-grained sandstones and thin coal beds. The distal braid-delta sediments, which include linguoid bars, inter-channel bay and splay deposits, are dominantly composed of medium- to coarse-grained, moderately sorted sandstones containing some thin mudstone intercalations. The medial braid-delta clastics include massive and trough-cross-bedded conglomerates and pebbly, trough- and planar-cross-bedded, very coarse-grained, poorly sorted sandstones.

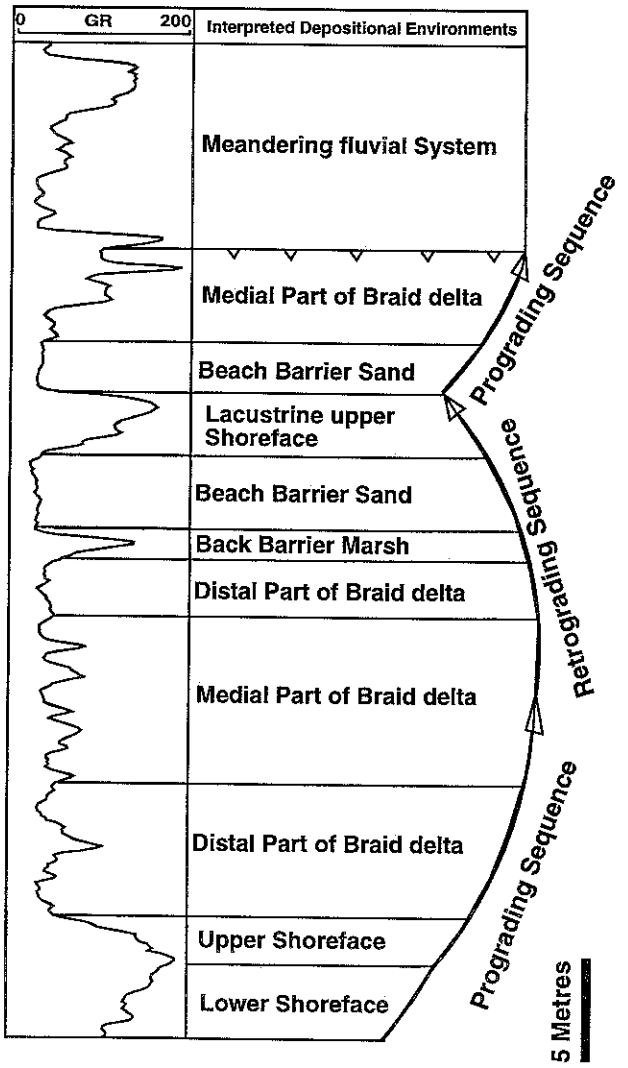

Figure 5. An example of the different depositional environments with progradational and retrogradational cycles of the Tirrawarra Sandstone in the Moorari and Fly Lake fields. The gamma ray log trace is derived from the Moorari-9 well.

The meandering system is composed of matrix-supported, oligomictic gravel lags, medium-grained, well-sorted, point-bar quartzarenites, and floodplain mudstone and coals. The aeolian beds are thin, medium-grained, supermature quartzarenites that formed on the point-bar sands during times of low water discharge.

The vertical succession in the Tirrawarra Sandstone around the Moorari and Fly Lake fields (Fig. 5) records progradation and retreat of a braid delta in a lacustrine environment. The lower Tirrawarra Sandstone starts with a progradational sequence that is overlain by a retrogradational sequence, then another progradational sequence. The remaining upper part of the unit displays a sudden change in sedimentary environment from a braided to meandering environment. The boundary is marked by a thin, widespread conglomerate with an erosional lower contact which suggests a hiatus (T0). This unconformity coincides with the unconformity in the Tirrawarra Field suggested by Seggie *et al.* (1994).

5. General diagenetic characteristics

The Tirrawarra Sandstone in the Moorari and Fly Lake fields consists mainly of medium-grained, moderately sorted sublitharenites (classification of Folk, 1974). A variety of authigenic minerals are recognized, including syntaxial quartz overgrowths, minor illite, patchy kaolin and siderite. Attention is focused on the siderite, and only a short description of the other diagenetic minerals is provided here.

Quartz is the dominant pore-filling cement in most samples. CL studies indicate at least six stages of quartz cement, although three main phases are distinguished (Z1–Z3). Homogenization temperatures of fluid inclusions entrapped within the quartz cement indicate that quartz cement precipitated at temperatures between 65 and 130 °C, unless the fluid inclusions re-equilibrated during burial (cf. Osborne & Haszeldine, 1993; Haszeldine & Osborne, 1993). Loose packing of framework grains shows that quartz cementation was initiated prior to major compaction but probably continued until relatively recent times.

Pore-filling euhedral and vermiform kaolin booklets are common and are sometimes intergrown with the outer margins of quartz overgrowths. Much of the kaolin is believed to have formed as a replacement product of feldspars and micas, although larger, more euhedral crystals, thought to be dickite, may have formed by slow precipitation from solution (cf. Loughnan & Roberts, 1986; Schulz-Rojahn & Phillips, 1989).

The authigenic nature of the illite is evident from its fibrous, lath- or lettuce-like habit. The mineral is thought to have formed as a replacement product of unstable rock fragments.

The siderite cementation and dissolution events occurred between, and synchronous with, other diagenetic processes, including quartz cementation, feldspar dissolution and kaolinization (Fig. 6). An early Fe-rich

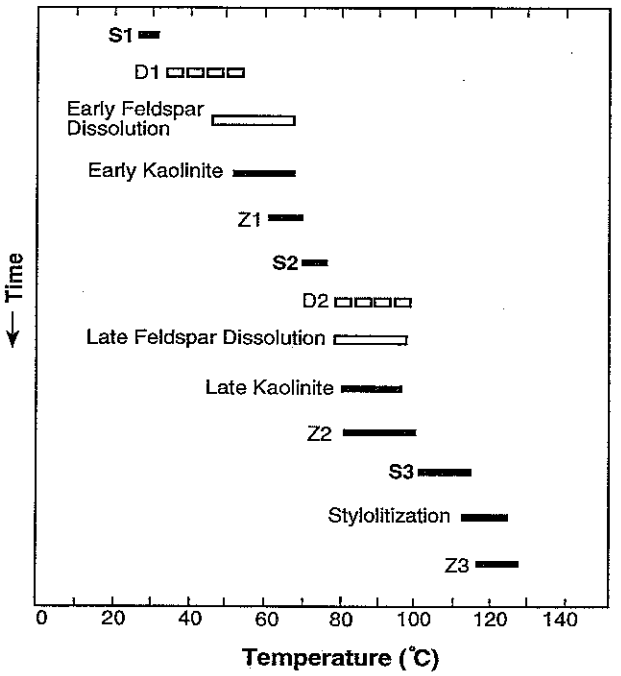

Figure 6. Generalized paragenetic sequence for the Tirrawarra Sandstone in the Fly Lake–Moorari area, Cooper Basin. The interpretation is based on the integration of petrographic, isotope and fluid inclusion results. S1 = early stage of siderite cement; S2 = middle stage of siderite cement; S3 = late stage of siderite cement; D1 and D2 = first and second main stages of siderite dissolution respectively; Z1 = innermost zone of brown-luminescing quartz cement; Z2 = middle zone of bright blue-luminescing quartz cement; Z3 = outer zone of brown-luminescing quartz cement.

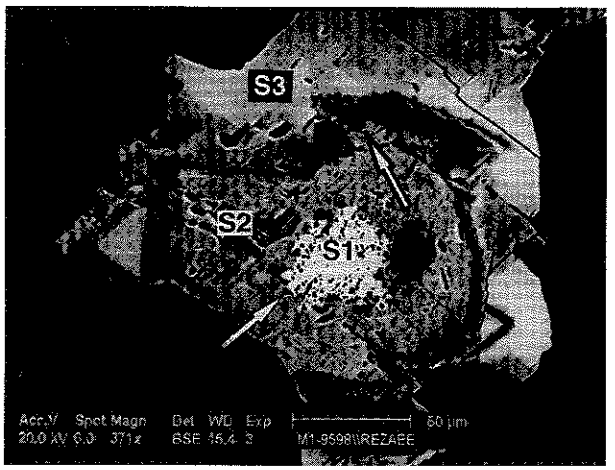

Figure 7. Back scatter electron (BSE) image showing the main siderite cement stages. S1 is white while the surrounding S2 is medium grey with variable internal composition, common pitting and complex zoning. S3 starts with regular banding, surrounded by a thick homogeneous zone of late-stage, pore-filling cement. Arrows point to irregular dissolution boundaries, between S1 and S2 and between S2 and S3. The cement relationships are typical of the Tirrawarra Sandstone. Sample M1-9598, Moorari-1, 2925.5 m. Scale bar = 50 µm.

siderite precipitated during methanogenesis whilst later, Mg-rich cement stages formed at elevated temperatures from carbon produced mainly from maturing hydrocarbon source rocks (Rezaee & Schulz-Rojahn, 1996).

6. Siderite cement characteristics

Siderite cement occurs in varying proportions in the Tirrawarra Sandstone and constitutes up to about 30 % of rock composition in some samples, as determined by point-counting. Under the petrographic microscope, siderite is generally seen as isolated, sparry rhombs or as a pore-filling cement, although a variety of different crystal habits are apparent, including rhombohedral, blocky and radial forms. Both petrographic and XRD results suggest a single-phase cement and only rarely is a more complex siderite cement evident under the petrographic microscope. When viewed under the electron microprobe and using BSE imaging techniques, however, three main stages of siderite cement are identified, including an early (S1), middle (S2) and late stage cement (S3) (Fig. 7). Fluid inclusion data indicate that the different siderite cement stages precipitated under different temperature conditions.

6.a. Early stage of siderite cement (S1)

Under the optical microscope, S1 is of a blotchy appearance, displays a moderately light to dark brown colour and appears devoid of fluid inclusions. In some samples, S1 is the only siderite cement, especially in fine-grained, poorly sorted marsh sediments, rich in organic matter. In samples where S1 completely cements the rock, quartz grains are characterized by a very loose grain packing, with individual grains floating in the siderite matrix. Where other siderite cement stages are present, S1 generally represents the substrate or nuclei for the middle stage of siderite cement precipitation (S2) (Fig. 7). The boundary between S1 and S2 is not always distinct but typically is characterized by irregular and serrated edges, indicating partial dissolution of S1 prior to S2 cementation (Fig. 7). In a BSE image, S1 is white and appears homogeneous. Electron microprobe analysis for S1 shows a high Fe/Mg ratio. The average composition of S1 is $(Fe_{96\%}Mg_{1\%}Ca_{1.7\%}Mn_{1.3\%})CO_3$. In samples which contain the highest proportion of S1, oxygen isotope compositions range from 13.9‰ to 15‰, with a mean $\delta^{13}C$ of +1.45‰ (Tables 2, 3).

6.b. Middle stage of siderite cement (S2)

In BSE images, S2 occurs as rhombs which generally enclose S1 (Figs 7–10) and which are, in turn, often engulfed by S3. Differentiation between S2 and S3 is difficult under the optical microscope except where small dissolution pits occur on the boundary between S2 and S3. S2 is characterized by many small (3–5 µm) primary fluid inclusions and common dissolution pits while S3

Table 2. Carbon and oxygen isotope data of the Tirrawarra Sandstone siderite cements

Well name	Sample	$\delta^{13}C$ (PDB‰)	$\delta^{18}O$ (SMOW‰)
Moorari 5	M5-9583	-10.37	6.6
Moorari 2	M2-10145	-11.13	6.15
Moorari 4	M4-9574	-10.68	8.59
Moorari 7	M7-9606	-10.49	7.28
Moorari 2	M2-10116	-8.13	10.86
Fly Lake 1	F1-9417	-3.83	14.18
Moorari 6	M6-9737	-9.70	11.19
Fly Lake 1	F1-9431	-4.22	11.48
Moorari 1	M1-9598	-7.07	12.42
Moorari 3	M3-9440	-5.98	14.61
Fly Lake 2	F2-9583	1.45	14.14
Moorari 3	M3-9503	-7.97	12.31
Moorari 1	M1-9613	-9.22	11.75
Moorari 4	M4-9554	-8.95	12.81
Moorari 9	M9-9732	-4.99	14.27
Moorari 3	M3-9422	-3.87	15.13
Moorari 1	M1-9620	-6.23	13.28
Fly Lake 4	F4-9441	1.46	13.97

Table 3. Summary table showing the isotope, compositional and fluid inclusion characteristics of the main siderite cement stages (S1, S2, S3)

	S1	S2	S3
$\delta^{18}O$ (‰ SMOW)	15	12	6
$\delta^{13}C$ (‰ PDB)	1.45	–8.5	–11
Th (C)	–	68	102
FeO (%)	96	74	75.5
MgO (%)	1.0	24	23
CaO (%)	1.7	0.8	0.5
MnO (%)	1.3	1.2	1.0

Th = fluid inclusion homogenization temperature.

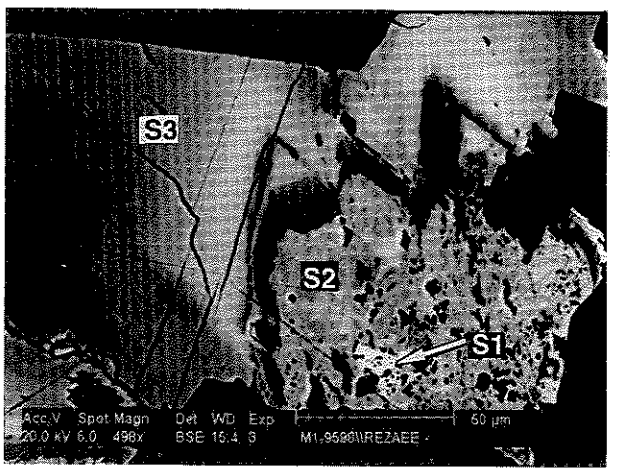

Figure 8. In this BSE image, homogeneous S3 siderite is the main pore-filling cement. There is a distinct dissolution boundary between S2 and S3 with dissolution pits in S2. There are isolated remnants of white S1 within S2. Dark banding early in the S3 cement shows euhedral rhombic terminations of crystals that grew on the dissolution surface on S2. Sample M1-9598. Moorari-1, 2925.5 m. Scale bar = 50 µm.

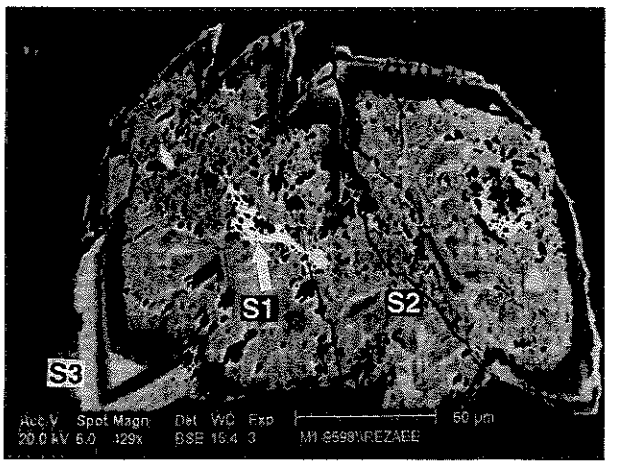

Figure 9. The BSE image shows patchy, isolated, white remnants of S1 within the medium grey, inhomogeneous and complexly zoned S2. The bulk of the area of cement is enclosed in a thin rim euhedral S3 cement with well-defined compositional banding. Dissolution features include pitting within S2 and the irregular boundary between S2 and S3. Sample M1-9598, Moorari-1, 2925.2 m. Scale bar = 50 µm.

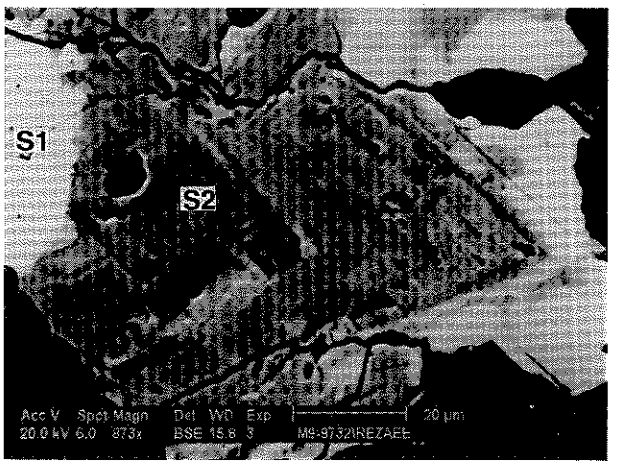

Figure 10. BSE image showing light grey, remnant S1 cement with dissolution edges engulfed by abundant dark grey S2 cement that displays complex compositional variation, irregular zoning and pitting. Sample M9-9732, Moorari-9, 2966.3 m. Scale bar = 50 µm.

has fewer inclusions. Locally, S2 is engulfed by quartz cement, indicating that some quartz cementation postdates S2 precipitation. In BSE images, S2 displays a distinct irregular compositional zoning (Figs 10, 11), indicating pore fluid chemistry fluctuations occurred during cementation. Similar zonation is completely absent in S1.

Based on grey-scale characteristics, three main zones, dark, moderate and light, are evident in S2. Electron microprobe analyses reveal different elemental compositions and variable substitution of Mg in each of the S2 sub-stages (Table 1). S2 compositions range from

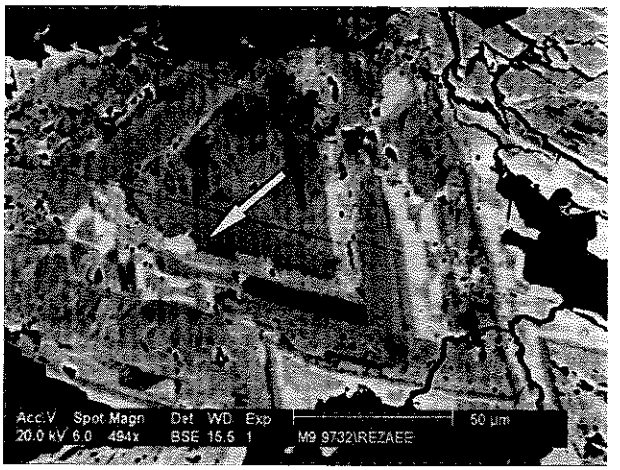

Figure 11. BSE image of S2, the middle stage of siderite cement, showing rapid, irregular compositional zoning and minor dissolution (arrowed). Sample M9-9732, Moorari-9, 2966.3 m. Scale bar = 50 µm.

$(Fe_{87.2\%}Mg_{9.5\%}Ca_{0.7\%}Mn_{2.6\%})CO_3$ to $(Fe_{56.7\%}Mg_{42.2\%}Ca_{0.15\%}Mn_{0.95\%})CO_3$, with the average composition being $(Fe_{74\%}Mg_{24\%}Ca_{0.8\%}Mn_{1.2\%})CO_3$ (Fig. 12) suggestive of sideroplesite for the light zone and pistomsite for the moderate to dark zone (classification of Deer, Howie & Zussman, 1992). In samples in which S2 is the dominant carbonate cement phase, oxygen isotope values range from 12.2‰ to 12.7‰ whilst the mean $\delta^{13}C$ composition is –8.5‰ (Tables 2, 3). Homogenization temperatures of S2 fluid inclusions range from 66 to 76 °C, with a median of around 68 °C (Fig. 13).

6.c. Late stage of siderite cement (S3)

Under the optical microscope, S3 is a blocky, colourless, very clear cement, post-dating S1 and S2. The boundary between S2 and S3 is characterized by an irregular, serrated outline, implying partial dissolution of S2 prior to precipitation of S3. In some samples, dead oil concentrates in fluid inclusions on the boundary between S2 and S3, indicating that hydrocarbon migration occurred synchronous with, or after the dissolution event but prior to S3 precipitation. BSE images show that S3 commences with regular dark and light banding which is then followed by a thick homogeneous cement phase. The early S3 bands are characterized by a high Mg content (pistomsite) and this grades into a relatively thick, homogeneous sideroplesite cement (Figs 7–9). Electron microprobe analyses indicate extensive substitution of Mg, with an average composition of $(Fe_{75.5\%}Mg_{23\%}Ca_{0..5\%}Mn_{1\%})CO_3$ for S3 (Fig. 12). Mean oxygen and carbon isotope values for samples in which S3 is the dominant carbonate cement are about 6‰ and –11‰ respectively (Tables 2, 3). Fluid inclusion results for S3 indicate a homogenization temperature of between 98 and 114 °C, with a median of about 102 °C (Fig. 13).

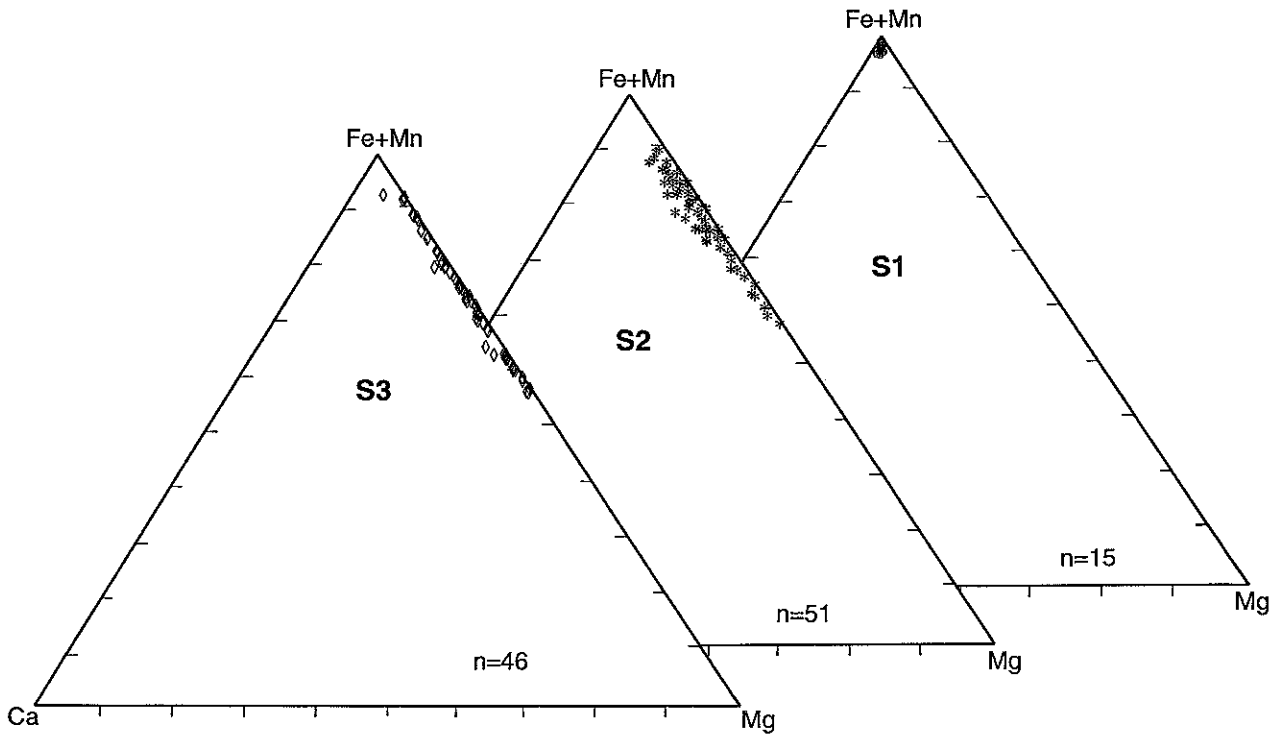

Figure 12. Ternary diagrams showing the relative proportions of Fe, Mn, Mg and Ca in the different stages of siderite cement in the Tirrawarra Sandstone. The early stage, S1, is very rich in Fe whereas the middle S2 and later S3 stages show substitution of Mg for Fe and fall within the realm of sideroplesite and pistomsite. S2 and S3 have almost identical compositions except that S2 has slightly higher Ca content.

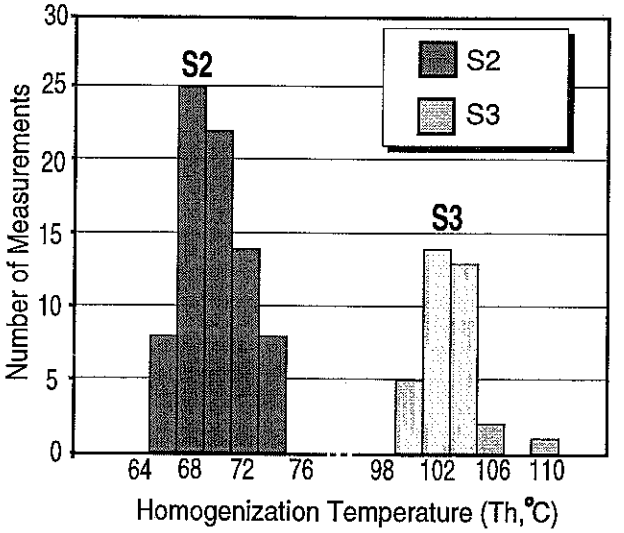

Figure 13. Fluid inclusion homogenization temperatures for the middle, S2, and late, S3, stages of Tirrawarra Sandstone siderite cements. S2 formed at much lower temperatures than S3. The early S1 siderite cement is devoid of visible fluid inclusions.

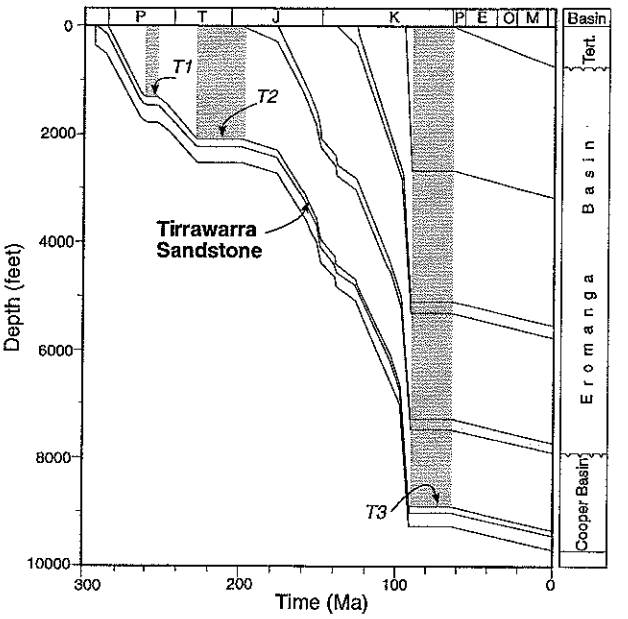

Figure 14. Burial history plot of Fly Lake-1 generated using BasinMod software. This is a simple plot with no erosion. Time breaks in the mid-Permian, late Triassic and late Cretaceous are shown as flat zones of non-deposition.

7. Thermal history modelling and the timing of siderite cements

Modelling was carried out using BasinMod 4.20 on a Sun workstation using the Lawrence Livermore National Laboratories vitrinite calculation option. Open-file vitrinite data were supplied by Santos Ltd. and Mines and Energy South Australia (MESA). Vitrinite values were calculated using a constant-heat-flow model calibrated on a surface temperature of 25 °C and a mean corrected bottom hole temperature (BHT) for the Fly Lake Field of 130 °C.

Various thermal scenarios were modelled using vitrinite data in order to constrain the timing of the siderite cements in the Tirrawarra Sandstone. In a simple thermal model with a constant (present) heatflow and without erosion at unconformities, the dominant feature in the thermal history is Cretaceous burial which caused rapid heating of the Tirrawarra Sandstone, forcing it into the oil window (Fig. 14). The temperatures from this simple model have been transferred onto Figure 15 and are shown as the solid line. Model vitrinite values are close to those measured at the level of the Tirrawarra Sandstone.

Figure 15 shows a schematic time–temperature path for the Tirrawarra Sandstone based upon thermal modelling. In this history, erosion occurred prior to 200 Ma but the maximum temperature was not achieved at that time. Near maximum temperatures are suggested to have occurred prior to late Cretaceous erosion. As there is no known recent subsidence, the present maximum temperature of 130 °C indicates a recent increase in geothermal gradient to 36 °C/km (Russell & Bone, 1989). This is large enough to have brought previously immature hydrocarbon source rocks to generation and expulsion.

The three main tectonic events which resulted in uplift and erosion in the Cooper Basin area are illustrated on the time–temperature path of the Tirrawarra Sandstone as T1, T2, and T3 (Fig. 15). The grey lines indicate the constraints implied by the homogenization temperatures of each siderite phase with two possibilities for timing of S2. Time B is based on a simple history with no uplift and time A takes account of event T2.

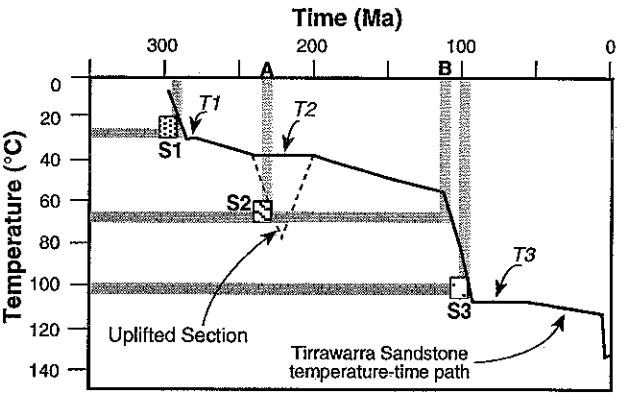

Figure 15. Schematic thermal history of the Tirrawarra Sandstone from the Fly Lake Field. The solid black line is the time–temperature profile derived from the simple geohistory plot in Figure 14 with no erosion taken into account. The horizontal grey lines are the temperature constraints derived from each of the S1, S2 and S3 stages of siderite cement. The intersection with the time–temperature path provides timing of each cement. S1 falls prior to tectonic event T1. Using the simple plot, S2 would plot at position B but dissolution edge and pitting on that phase suggests it formed prior to event T2. This requires late Triassic deposition then erosion of about 550 m. The temperature of S3 places it around 100 Ma, just prior to event T3.

8. Discussion

Consideration of BSE images and electron microprobe results have led to the identification of a multi-stage, pore-filling siderite cement in the Tirrawarra Sandstone of the Moorari and Fly Lake fields. Although previous workers had identified several siderite cement morphologies, they had considered the pore-filling sparry siderite to be a single-stage precipitate in Cooper Basin sediments (Martin & Hamilton, 1981; Schulz-Rojahn & Phillips, 1989).

Results from the present investigation show that the pore-filling siderite precipitated in three main stages in the Moorari–Fly Lake area. An early, homogeneous Fe-rich siderite (S1) was followed by a generally more extensive cement stage characterized by a complex compositional zoning (S2), and in turn was engulfed by a late-stage simply zoned to homogeneous siderite cement (S3).

Detailed observation of BSE images of S2 and S3 indicate two different hydraulic conditions in the reservoir. S2 shows irregular compositional zoning (Fig. 10), which indicates fluctuation in pore fluid chemistry. Minor dissolution evident between the patchy zonation (Fig. 11), shows that fluctuations in pore water chemistry were significant. Waves of varying geochemical concentration may be unrelated to tectonic activity but complex zoning with incipient dissolution suggests more severe fluctuation in what may be termed a hydraulically active porous medium. S3, however, displays a relatively consistent composition with simple zoning and no internal dissolution (Figs 8, 9). This indicates a more constant pore fluid chemistry suggestive of a hydraulically stable system.

8.a. Precipitation temperatures of siderite cement stages

The compositional zoning evident in S2 and S3 (Figs 7–11) indicates that the cements precipitated from solution and did not undergo recrystallization during burial diagenesis. No unstable precursor for siderite is known, and there exists no documented case of siderite recrystallization (Mozley & Carothers, 1992). For these reasons, fluid inclusions are thought to provide a genuine record of the temperatures at which the Tirrawarra Sandstone siderites crystallized, unless stretching of the inclusions (Osborne & Haszeldine, 1993; Haszeldine & Osborne, 1993) did occur. Consistent differences in homogenization temperatures between S2 and S3 in the same samples, however (Fig. 13), suggest the fluid inclusion data were not influenced by the stretching which affects mainly larger fluid inclusions (Osborne & Haszeldine, 1993; Haszeldine & Osborne, 1993).

In the study area, no appreciable differences in the size of the fluid inclusions were detected between S2 and S3. Present temperatures at reservoir level exceed the maximum homogenization temperatures of S3 by at least 20–30 °C, indicating that the fluid inclusions were not reset during recent geological times. Thermal modelling for the Cooper Basin shows that sediments did not undergo major subsidence in the last few million years in the Patchawarra Syncline (Tupper & Burckhardt, 1990). The homogenization temperatures of siderite can therefore be used to determine the $\delta^{18}O$ of the original pore water from which S2 and S3 precipitated.

The fluid inclusion data indicate that S2 precipitated at a mean water temperature of about 68 °C whilst S3 formed at about 102 °C (Fig. 13). The crystallization temperatures of S1 cannot be determined since no fluid inclusion data are available, but the cement stratigraphy would suggest it was lower than the temperature conditions for S2, that is, less than about 68 °C. Major differences in isotope composition between S1 and the later cement stages probably indicate that S1 precipitated at a considerably lower temperature than S2.

The palaeolatitude of central Australia during early Permian times was about 70–75° S (McElhinny, 1969; Embleton & McElhinny, 1982; Veevers, 1984). The $\delta^{18}O$ of recent meteoric water is between –15 and –16 per mil at this latitude (Dansgaard, 1964). Accordingly, using an intermediate $\delta^{18}O$ value of –15.5 per mil for early Permian pore water and using the isotope fractionation equation of Carothers, Adami & Rosenbauer (1988), it is suggested that S1 precipitated at a temperature of about 30 °C.

8.b. Dissolution events

Two periods of dissolution occurred between precipitation of different stages of siderite cement. The main dissolution boundaries almost certainly mark a time gap between the precipitation of each major stage of siderite cement, as is indicated by the different isotope compositions of the various cement stages.

The first dissolution event (D1) occurred between the precipitation of S1 and S2, at reservoir temperatures probably between about 30 and 68 °C as suggested by the stable isotope and fluid inclusion data. The second major dissolution phase (D2) took place after the formation of S2 but before S3 cementation, in the temperature range of about 68–102 °C, probably coinciding with the timing of hydrocarbon generation and migration in the studied area. Several minor dissolution phases also occur during precipitation of S2 (Fig. 11). The main dissolution events clearly record dramatic variations in the pore water chemistry, and it is suggested here that these may be related to the tectonic events which are known to have influenced the basin. The timing of the dissolution is constrained by correlation of the temperatures of precipitation of each phase with the time–temperature path derived from wells in the study area (Fig. 15).

While speculative, the following suggestions do provide a mechanism for the dissolution events. The first dissolution event (D1) may well have been triggered by tectonic activity which allowed invasion of low-pH meteoric pore waters. The presence of dead oil at the dissolution boundary between S2 and S3 may point toward the role of organic processes in triggering carbonate cement dissolution, prior to or synchronous with petroleum migration. The second dissolution phase (D2) broadly coincides with the temperature window for peak hydro-

carbon generation (Tissot & Welte, 1978). It is possible that organic acids which accompanied kerogen maturation (Schmidt & McDonald, 1979; Surdam, Boese & Crossey, 1984; Burley, 1986) triggered the dissolution event. According to Curtis (1983), maturing kerogen can generate Al-bearing acidic pore water that produces late-stage kaolin. In the Tirrawarra Sandstone, either meteoric invasion or source-rock maturation probably accounts for the association of authigenic kaolin patches with siderite spar displaying partial dissolution.

8.c. Burial history and siderite cement stages

Plotting different stages of siderite cement on the time–temperature path of the Tirrawarra Sandstone (Fig. 14), constrains the timing of cement precipitation and dissolution, points to the influence of tectonic activity and allows the burial history to be further refined.

The grey lines on Figure 15 illustrate the constraints implied by the cement precipitation temperatures. S1 was precipitated prior to the uplift T1. S2, with precipitation temperatures from 66–72 °C, would fall on the time–temperature curve around 110 Ma (position B on Fig. 15) if the burial history was a simple one with no uplift. This would place S2 very close to S3 with no obvious reason for the dissolution event between them. It is suggested that S2 was emplaced prior to the main uplift of T2, position A on Figure 15. This implies that additional section was deposited to allow the Tirrawarra Sandstone to reach around 70 °C prior to at least 550 metres of uplift and erosion.

The presence of minor dissolution phases between different zones of S2 and relatively rapid compositional zoning in this stage of siderite cement suggest that the formation of S2 occurred during unstable conditions, possibly during the onset of T2.

The precipitation temperature of the late stage of siderite cement (S3) shows that it formed around 100 Ma, probably before T3 (Fig. 15). S3 formed during relatively stable hydraulic conditions in the Cooper Basin as indicated by the regular zoning then thick homogeneous stage (Figs 7–9). This could be synchronous with the rapid burial stage in mid-Cretaceous time.

The first phase of dissolution (D1), which occurred at temperatures between 30 and 68 °C, is most likely have occurred during first tectonic event (T1) which may have allowed invasion of low-pH meteoric water into the reservoir. The second dissolution phase has occurred between 68 and 102 °C. The presence of dead oil at the dissolution boundary between S2 and S3 may point toward the role of organic processes in triggering S2 dissolution, prior to or synchronous with petroleum migration.

9. Conclusions

In the Tirrawarra Sandstone of the Cooper Basin, three stages of siderite cement have formed under different tectonic conditions:

(a) The early stage (S1) which formed about 30 °C is an Fe-rich structureless cement. S1 precipitated before the first tectonic event after deposition of Tirrawarra Sandstone.

(b) The middle stage of siderite cement (S2) which formed about 68 °C, was formed under tectonically active conditions in the Cooper Basin, probably in the lead up to T2. This stage of siderite cement is characterized with relatively rapid and irregular compositional zoning and minor dissolution phases.

(c) The late stage siderite cement (S3) which formed about 102 °C, is a cement formed under tectonically stable conditions in the Cooper Basin.

With the knowledge of precipitation temperature and timing of S2, it is possible to estimate the amount of erosion during T2. Assuming the current thermal gradient for the Patchawarra syncline of about 36 °C/km (Russell & Bone, 1989) was valid for T2 time, at least 550 metres uplift and erosion would have been required in the late Triassic in the study area. If S3 was precipitated at the near maximum burial depth at 102 °C, the current temperature of 130 °C indicates a recent increase in thermal gradient. Such a recent increase has major implications for thermal history modelling of the area and potentially a major impact on the hydrocarbon exploration task for the Patchawarra Syncline.

Acknowledgements. The authors thank Dr Peter Tingate for thermal modelling and useful discussions during the preparation of this paper. The manuscript was greatly improved by the constructive comments of *Geological Magazine* reviewers Drs R. S. Haszeldine and A. E. Fallick. The authors gratefully acknowledge financial support by NCPGG, the Australian Petroleum Cooperative Research Centre (APCRC), and Santos Ltd.

References

APAK, S. N., STUART, W. J. & LEMON, N. M. 1993. Structural-stratigraphic development of the Gidgealpa–Merrimelia–Innamincka Trend with implications for petroleum trap styles, Cooper Basin, Australia. *Australian Petroleum Exploration Association Journal* **33**, 94–104.

ARMSTRONG, J. D. & BARR, T. M. 1986. The Eromanga Basin. An overview of exploration and potential. *Geological Society of Australia Special Publication* **12**, 25–38.

BATTERSBY, D. G. 1976. Cooper Basin oil and gas fields. In *Economic Geology of Australia and New Guinea, 3* (eds R. B. Leslie, H. J. Evans and C. L. Knight), pp. 321–70. Australasian Institute of Mining and Metallurgy, Monograph no. 7.

BEVER, J. M., CARROLL, P. G., WILDE, E. & WILLIAMS, B. P. J. 1998. Core facies, petrology, and permeability of Tirrawarra Sandstone, Moorari Field, Cooper Basin, South Australia. *American Association of Petroleum Geologists Bulletin* **72**, 162.

BURLEY, S. D. 1986. The development and destruction of porosity within Upper Jurassic reservoir sandstones of the Piper and Tartan Fields, Outer Moray Firth, North Sea. *Clay Mineralogy* **21**, 649–94.

CAROTHERS, W. W., ADAMI, H. L. & ROSENBAUER, R. J. 1988. Experimental oxygen isotope-fractionation between siderite-water and phosphoric acid liberated CO_2-siderite. *Geochimica et Cosmochimica Acta* **52**, 2445–50.

CRAIG, H. 1957. Isotope standards for carbon and oxygen and correction factors for mass spectrometric analysis of carbon dioxide. *Geochimica et Cosmochimica Acta* **12**, 133–49.

CRAIG, H. 1961. Standards for reporting concentrations of deuterium and oxygen-18 in natural waters. *Science* **133**, 1833–4.

CURTIS, C. D. & COLEMAN, M. L. 1986. Controls on the precipitation of early diagenetic calcite, dolomite, and siderite concretions in complex depositional sequences. In *Roles of Organic Matter in Sediment Diagenesis* (ed. D. L. Gautier), pp. 23–33. SEPM Special Publication no. 38.

CURTIS, C. D. 1983. Link between aluminium mobility and destruction of porosity. *American Association of Petroleum Geologists Bulletin* **63**, 380–4.

CURTIS, C. D., PEARSON, M. J. & SOMOGYI, V. A. 1975. Mineralogy, chemistry, and origin of a concretionary siderite sheet (clay-ironstone band) in the Westphalian of Yorkshire. *Mineralogical Magazine* **40**, 385–93.

DANSGAARD, W. 1964. Stable isotopes in precipitation. *Tellus* **16**, 436–68.

DEER, W. A., HOWIE, R. A. & ZUSSMAN, J. 1992. *An introduction to the rock-forming minerals*. London: Longman Group Limited, 695 pp.

EMBLETON, B. J. J. & MCELHINNY, M. W. 1982. Marine magnetic anomalies, palaeomagnetism and the drift history of Gondwanaland. *Earth and Planetary Science Letters* **58**, 141–50.

EXON, N. F. & SENIOR, B. R. 1976. The Cretaceous of the Eromanga and Surat Basins. *BMR Journal of Australian Geology and Geophysics* **1**, 33–50.

FAIRBURN, W. A. 1989. The geometry of Toolachee unit 'C' fluvial sand trends, Moomba Field, Permian Cooper Basin, South Australia. *Australian Petroleum Exploration Association Journal* **29**, 239–50.

FOLK, R. L. 1974. *Petrology of sedimentary rocks*. Austin, Texas: Hemphill Publishing Co., 182 pp.

GATEHOUSE, C. G. 1972. Formations of the Gidgealpa Group in the Cooper Basin. Aust. *Oil & Gas Journal* **18**, 10–15.

GATEHOUSE, C. G. 1986. The geology of the Warburton Basin in South Australia. *Australian Journal of Earth Science* **33**, 161–80.

GAUTIER, D. L. 1982. Siderite concretions: indicators of early diagenesis in the Gammon Shale (Cretaceous). *Journal of Sedimentary Petrology* **52**, 859–71.

GRAY, R. J. & ROBERTS, D. C. 1984. A seismic model of faults in the Cooper Basin. *Australian Petroleum Exploration Association Journal* **24**, 421–8.

HASZELDINE, R. S. & OSBORNE, M. 1993. Fluid inclusion temperatures in diagenetic quartz reset by burial: implications for oil field cementation. In *Diagenesis and Basin Development* (eds A. D. Horbury and A. G. Robinson), pp. 35–46. AAPG Studies in Geology no. 36.

HEATH, R. 1989. Exploration in the Cooper Basin. *Australian Petroleum Exploration Association Journal* **29**, 366–78.

HILL, A. J. & GRAVESTOCK, D. I. 1995. Cooper Basin. In *The Geology of South Australia, Volume 2, The Phanerozoic* (eds J. F. Drexel and W. V. Preiss), pp. 78–87. South Australian Geological Survey, Bulletin no. 54.

HUNT, J. W., HEATH, R. S. & MCKENZIE, P. F. 1989. Thermal maturity and other geological controls on the distribution and composition of Cooper Basin hydrocarbons. *Australian Petroleum Exploration Association Journal* **29**, 509–23.

KANTSLER, A. J., PRUDENCE, T. J. C., COOK, A. C. & ZWIGULIS, M. 1983. Hydrocarbon habitat of the Cooper/Eromanga Basin. *Australian Petroleum Exploration Association Journal* **23**, 373–89.

KAPEL, A. J. 1966. The Cooper's Creek Basin. *Australian Petroleum Exploration Association Journal* **6**, 71–5.

KAPEL, A. J. 1972. The geology of the Patchawarra area Cooper Basin. *Australian Petroleum Exploration Association Journal* **12**, 53–7.

KREIG, G. W., ALEXANDER, E. M. & ROGERS, P. A. 1995. Eromanga Basin. In *The Geology of South Australia, Volume 2, The Phanerozoic* (eds J. F. Drexel and W. V. Preiss), pp. 101–5. South Australian Geological Survey, Bulletin no. 54.

LOUGHNAN, P. F. & ROBERTS, F. I. 1986. Dickite- and kaolinite-bearing sandstones and conglomerates in Illawarra Coal Measures of the Sydney Basin, New South Wales. *Australian Journal of Earth Science* **33**, 325–32.

MARTIN, K. R. & HAMILTON, N. J. 1981. Diagenesis and reservoir quality, Toolachee Formation, Cooper Basin. *Australian Petroleum Exploration Association Journal* **21**, 143–54.

MCCREA, J. M. 1950. On the isotopic chemistry of carbonates and a palaeotemperature scale. *Journal of Chemical Physics* **18**, 849–57.

MCELHINNY, M. W. 1969. The palaeomagnetism of the Permian of southeast Australia and its significance regarding the problem of intercontinental correlation. *Geological Society of Australia Special Publication* **2**, 61–7.

MOZLEY, P. S. & CAROTHERS, W. W. 1992. Elemental and isotopic composition of siderite in the Kuparuk Formation, Alaska: effect of microbial activity and water/sediment interaction on early pore-water chemistry. *Journal of Sedimentary Petrology* **62**, 681–92.

OSBORNE, M. & HASZELDINE, R. S. 1993. Fluid inclusions in diagenetic quartz record oilfield burial temperatures, not precipitation temperatures. *Marine and Petroleum Geology* **10**, 271–8.

PEARSON, M. J. 1985. Some chemical aspects of digenetic concretions from the Westphalian of Yorkshire, England. *Chemical Geology* **31**, 225–44.

PYECROFT, M. 1973. The Della Field, Cooper Basin, South Australia. *Australian Petroleum Exploration Association Journal* **13**, 58–67.

REYNOLDS, T. J. 1978. *Fluid inclusion adapted U.S.G.S. gas flow heating/freezing instruction manual*. Denver: Fluid Incorporated.

REZAEE, M. R. & SCHULZ-ROJAHN, J. P. 1996. Application of quantitative back-scattered electron image analysis in isotope interpretation of siderite cement: Tirrawarra sandstone reservoir, Cooper Basin (Australia) In *Carbonate Cementation in Sandstones* (ed. S. Morad). International Association of Sedimentologists Special Publication, in press.

RODDA, J. S. & PASPALIARIS, T. G. 1989. Tirrawarra and Moorari Oil Fields enhanced oil recovery schemes – further developments. *Australian Petroleum Exploration Association Journal* **29**, 121–30.

ROSENBAUM, J. & SHEPPARD, S. M. F. 1986. An isotopic study of siderites, dolomites and ankerites at high temperatures. *Geochimica et Cosmochimica Acta* **50**, 1147–50.

RUSSELL, N. J. & BONE, Y. 1989. Palaeogeothermometry of the Cooper and Eromanga Basins, South Australia. *Australian Petroleum Exploration Association Journal* **29**, 559–81.

SCHMIDT, V. & MCDONALD, D. A. 1979. The role of secondary porosity in the course of sandstone diagenesis. *SEPM Special Publication* **26**, 175–207.

SCHULZ-ROJAHN, J. P. & PHILLIPS, S. E. 1989. Diagenetic alteration of Permian reservoir sandstones in the Nappamerri

Trough and adjacent areas, southern Cooper Basin. *Australian Petroleum Exploration Association Journal* **29**, 629–45.

SEGGIE, R. J. LANSOM, P. B. HAMLIN, H. S. & JOHNSON, G. A. 1994. The Tirrawarra oil field: Field revitalisation through reservoir description and characterisation. *Australian Petroleum Exploration Association Journal* **34**, 33–54.

SMYTH, M. 1979. Hydrocarbon generation in the Fly Lake-Brolga area of the Cooper Basin. *Australian Petroleum Exploration Association Journal* **19**, 108–14.

STANLEY, D. J. & HALLIDAY, G. 1984. Massive hydraulic fracture stimulation of Early Permian gas reservoirs, Big Lake Field, Cooper Basin, *Australian Petroleum Exploration Association Journal* **24**, 180–195

STUART, W. J. 1976. The genesis of Permian and Lower Triassic reservoir sandstones during phases of southern Cooper Basin development. *Australian Petroleum Exploration Association Journal* **16**, 37–47.

STUART, W. J., KENNEDY, S. & THOMAS, A. D. 1988. The influence of structural growth and other factors on the configuration of fluviatile sandstones, Permian Cooper Basin. *Australian Petroleum Exploration Association Journal* **28**, 255–66.

SURDAM, R. C., BOESE, S. W. & CROSSEY, L. J. 1984. The chemistry of secondary porosity. In *Clastic Diagenesis* (eds D. A. McDonald and R. C. Surdam), pp. 127–49. American Association of Petroleum Geology Memoir no. 37.

THORNTON, R. C. N. 1978. Regional lithofacies and palaeogeography of the Gidgealpa Group. *Australian Petroleum Exploration Association Journal* **18**, 52–63

THORNTON, R. C. N. 1979. Regional stratigraphic analysis of the Gidgealpa Group, Southern Cooper Basin, Australia. *Geological Survey of South Australia Bulletin* **49**, 1–140.

TISSOT, B. P. & WELTE, D. H. 1978. *Petroleum formation and occurrence – a new approach to oil and gas exploration.* Berlin: Springer Verlag, 538 pp.

TUPPER, N. P., BURCKHARDT, D. M. 1990. Use of the methylphenanthrene index to characterise expulsion of Copper and Eromanga Basin oils. *Australian Petroleum Exploration Association Journal* **30**, 373–85.

VEEVERS, J. J. 1984. *Phanerozoic earth history of Australia.* Oxford Geological Science Series. New York: Oxford University Press, 418 pp.

WILLIAMS, B. P. J., WILD, E. K. & SUTTILL, R. J. 1985. Paraglacial aeolianites: potential new hydrocarbon reservoirs, Gidgealpa Group, southern Cooper Basin. *Australian Petroleum Exploration Association Journal* **25**, 291–310.

WOPFNER, H. 1966. A case history of the Gidgealpa Gas Field, South Australia. *Australian Oil & Gas Journal* **12**, 29–53.

YEW, C. C. & MILLS, A. A. 1989. The occurrence and search for Permian oil in the Cooper Basin, Australia. In *The Cooper and Eromanga Basins, Australia* (ed. B. J. O'Neil), pp. 339–59. Proceedings PESA/SPE/ASEG Conference, Adelaide.